In: Plasma Physics and Controlled Fusion 1999. Vol. 41, pp. 1231-1249.
Reprinted with permission from the publisher.
http://www.iop.org/journals/ppcf

Plasma Phys. Control. Fusion **41** (1999) 1231–1249. Printed in the UK PII: S0741-3335(99)03721-5

Role of fast waves in the central deposition of lower hybrid power

J A Heikkinen†, T J J Tala‡, T J H Pättikangas†, A D Piliya§, A N Saveliev§ and S J Karttunen†

† Association Euratom–Tekes, VTT Energy, PO Box 1604, FIN-02044 VTT, Finland
‡ Association Euratom–Tekes, Helsinki University of Technology, Advanced Energy Systems, PO Box 2200, FIN-02015 HUT, Finland
§ A F Ioffe Physical Technical Institute, Politekhnicheskaya ul. 26, 194021, St Petersburg, Russian Federation

Received 26 April 1999, in final form 20 July 1999

Abstract. In tokamaks, lower hybrid (LH) waves are routinely used for current drive and heating of plasmas. The LH waves have two modes of propagation that are called the slow and the fast wave. Usually, the lower hybrid waves are launched as slow waves into a tokamak, but during the propagation part of the wave power can be transformed to fast waves. General characteristics of the mode transformation of slow waves to fast waves are first investigated with a simple quasitoroidal ray-tracing model. Next, the effect of mode transformed LH power on the deposition profiles in a JET-like tokamak is analysed by using the fast ray-tracing code FRTC. When the launched spectrum is at small values of the toroidal refractive index ($1.6 \lesssim n_{\phi 0} \lesssim 2.0$), the contribution of the fast wave to the deposited power is found to be significant and responsible for most of the absorption at the centre. When $n_{\phi 0}$ is large ($n_{\phi 0} \gtrsim 2.2$), the effect of the mode transformed fast waves is small or negligible. At modest central densities ($n_{e0} \sim 0.5 \times 10^{20}$ m^{-3}), the contribution of the fast wave to the power deposition can be more than 50% in the plasma centre. In consequence, the significant amount of wave energy absorbed in the fast mode must be carefully taken into account in modelling LH current drive experiments in the future. At low central densities ($n_{e0} \lesssim 0.3 \times 10^{20}$ m^{-3}), practically no absorption of fast waves occurs.

1. Introduction

Radiofrequency (RF) power in the lower hybrid (LH) range of frequencies plays an important role in profile control and non-inductive current drive of the present tokamak devices. It is well known that RF power in this frequency range can propagate in the form of two wave modes. These modes, called the slow and the fast waves, respectively, are different in their propagation and damping properties, their interaction with alpha particles and other fast ions is distinct, the fast waves do not possess any lower hybrid resonance and have a small $n_\parallel$ shift. In particular, since the Landau damping is much weaker for the fast wave, this mode is expected to provide more central power deposition and current generation in large tokamaks.

The type of wave mode is not, as a rule, conserved in the process of wave propagation. In certain conditions, it is changed via the linear mode conversion. As a result, LH waves excited in a tokamak represent a mixture of both modes regardless of the launching conditions. This feature of lower hybrid heating (LHH) and current drive (LHCD) is taken into account automatically in most modern ray-tracing codes. However, the relative role of the two wave modes has not been investigated in sufficient detail. Also, the possibility of optimizing the

launched $n_\parallel$ spectrum with regard to this phenomenon remains an open question. It is important to discuss the characteristic features of the fast–slow (slow–fast) linear mode conversion in a tokamak configuration and make comparisons with the better known case of slab geometry.

The accessibility of LH waves in a slab geometry is often expressed by a lower bound on the launched parallel refractive index $n_{\parallel 0}$ obtained from the well known condition [1]

$$n_{\parallel 0} \geqslant n_{\parallel c} \approx \sqrt{S} + \omega_{pe}^2/\Omega_e^2$$

where

$$S = 1 - \omega_{pi}^2/(\omega^2 - \omega_{ci}^2) - \omega_{pe}^2/(\omega^2 - \omega_{ce}^2)$$

ω_{pe} is the electron plasma frequency, Ω_e is the electron cyclotron frequency and ω is the wave angular frequency.

For $n_{\parallel 0} < n_{\parallel c}$, the slow wave launched by the antenna can transform to a fast wave before reaching the region where $n_{\parallel c}$ is evaluated. The fast wave can then return to outer plasma layers where it is reflected. On the other hand, if $n_{\parallel 0} > n_{\parallel c}$, the slow wave has access to the region where $n_{\parallel c}$ is evaluated. If damping is weak, the slow wave can make multiple passes with a consequent evolution of $n_\parallel$ and with a repeated possibility of transforming to a fast mode at $n_\parallel = n_{\parallel c}$.

The transformation to the fast mode has been known [2–8] to be possible for slow waves that have access to the tokamak plasma centre and launched with a toroidal refractive index $n_{\phi 0}$ spectrum extending below a certain threshold $n_{\phi 0}^\star$ [5, 6] in an interval of poloidal mode numbers m. The implications to power deposition and mode partition in the propagation region have not, however, been studied so far in detail. Moreover, it has been shown [3] that the fast waves resulting from mode transformation would preferentially propagate in the outer plasma layers, which leads to decreased power deposition in the plasma centre.

In the present paper, the characteristics and occurrence of mode transformation and its effect on the power deposition in LHCD are investigated. Both a cylindrical quasitoroidal approximation and a JET-type elongated toroidal configuration are considered. Rays launched in a slow mode are followed to resolve the evolution of the parallel refractive index, the poloidal mode number and the polarization as a function of launching parameters. The fast ray-tracing code FRTC [9] is applied to obtain ensemble-averaged power deposition for a number of launched $n_\parallel$ spectra. In contrast to previous understanding, the fast waves are found to contribute significantly to the power deposition and to constitute even half of the total absorption and most of the central absorption in the JET configuration with relevant $n_{\parallel 0}$ spectra.

In section 2, a general discussion and a short review of the mode transformation problem for the LH waves is given. Section 3 explains the conditions for mode transformation and the adopted ray-tracing equations within a quasitoroidal model. This simple quasitoroidal ray-tracing model includes only the correct propagation properties of LH waves in a torus, but no power absorption is calculated or considered. Section 4 describes the regions of accessibility for the slow and fast waves and the regimes where mode transformation can occur. Section 5 presents the FRTC results for ray ensembles showing the power deposition profiles for both slow and fast wave direct excitations. The results are discussed in section 6.

2. Physics of fast/slow wave transformation

Properties of waves in magnetized plasmas are strongly dependent on their parallel refractive index $n_\parallel$. Therefore, propagation of a wave mode can be analysed conveniently with a given value of this parameter. In a cold plasma, the dispersion relation reads

$$H = A(n_\parallel)n_\perp^4 + F(n_\parallel)n_\perp^2 + C(n_\parallel) = 0 \tag{1}$$

where $n_\perp$ is the perpendicular refractive index of the wave with respect to the magnetic field and the coefficients are defined as $A = S, -F = (S+P)(S-n_\parallel^2) - D^2$ and $C = P[(S-n_\parallel^2)^2 - D^2]$. Here, $P = \epsilon_{zz}$ and $\mathrm{i}D = \epsilon_{xy}$ and $S = \epsilon_{xx}$ with ϵ_{ik} being the element of the cold plasma dielectric tensor in the coordinate system with the z-axis along the magnetic field.

In the LH frequency region, we have $\Omega_\mathrm{i} \ll \omega \ll \Omega_\mathrm{e}$ and typically, $\omega_\mathrm{pe} \gg \omega$ where ω and Ω_i are the wave frequency and the ion cyclotron frequency, respectively. Then the coefficients in equation (1) are given approximately by $A \equiv S \simeq 1 + w - v/M$, $F \simeq v(S - n_\parallel^2 + w)$ and $C \simeq v(vw - n_\parallel^4)$ where $w = \omega_\mathrm{pe}^2/\Omega_\mathrm{e}^2$, $v = \omega_\mathrm{pe}^2/\omega^2$ and $M = m_\mathrm{i}/m_\mathrm{e}$ with m_i and m_e being the ion and the electron mass, respectively.

The LH resonance occurs at the frequency $\Omega_\mathrm{LH} = [\omega_\mathrm{pi}^2\Omega_\mathrm{e}\Omega_\mathrm{i}/(\omega_\mathrm{pi}^2 + \Omega_\mathrm{e}\Omega_\mathrm{i})]^{1/2}$. Below the resonance, at $\omega < \Omega_\mathrm{LH}$, equation (1) has an unambiguous solution $n_\perp(n_\parallel)$ which exists for $n_\parallel > 0$ in the interval $0 < n_\parallel < n_\mathrm{max}$, where $n_\mathrm{max} = (vw)^{1/4}$. This situation is illustrated in figure 1(*a*). The mode described by this root of the dispersion relation is known in the LH frequency region as the fast wave. It represents the high-frequency limit of the fast magnetosonic wave.

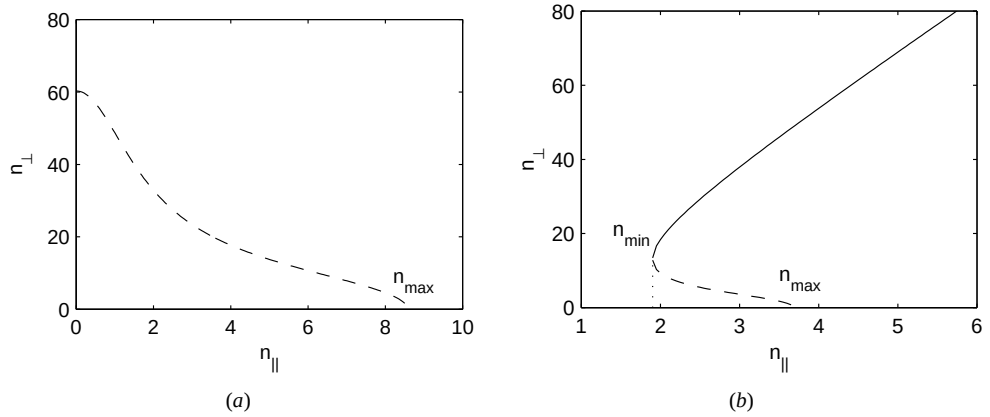

Figure 1. Dispersion curves for the fast wave (dashed curve) and the slow wave (full curve) when (*a*) $\omega < \Omega_\mathrm{LH}$ ($f = \omega/2\pi = 0.6$ GHz) and (*b*) $\omega > \Omega_\mathrm{LH}$ ($f = 3.7$ GHz). A deuterium plasma with $n_\mathrm{e} = 5 \times 10^{19}$ m^{-3} and $B = 3.2$ T is assumed. Since the left-hand side of equation (1) is an even function of both $n_\parallel$ and $n_\perp$, it is sufficient to consider solutions at positive values of these variables.

Above the LH resonance, the solution consists of two branches, as is shown in figure 1(*b*). The upper branch is called the slow wave and the lower branch is the fast wave. The lower branch exists in the interval $n_\mathrm{min} < n_\parallel < n_\mathrm{max}$, where n_min is found from the relation $F^2 - 4AC = 0$ as follows:

$$n_\mathrm{min} = w^{1/2} \pm S^{1/2}. \tag{2}$$

In addition to having different values of $n_\perp$, the slow and fast waves with the same $n_\parallel$ are different in their polarization. In particular, the slow mode is electrostatic at $n_\parallel^2 \gg 1$. In this limiting case, it is also known as the oblique electron plasma wave or the Trivelpiece–Gould mode.

In a weakly inhomogeneous plasma, equation (1) describes the slow and the fast WKB waves. Three different parameter regions exist for these waves at a given frequency ω. Firstly, if $\omega < (\Omega_\mathrm{e}\Omega_\mathrm{i})^{1/2}$, two modes can exist simultaneously in the region $1 < v < v_\mathrm{res}$, where v_res is the value of v at the LH resonance layer. Secondly, if $\omega > (\Omega_\mathrm{e}\Omega_\mathrm{i})^{1/2}$, two modes can exist at

any density $v > 1$. Thirdly, only the fast mode exists at $v > v_{\rm res}$. Considering the dependence of $n_\perp$ on the plasma density, one can see that $n_\perp \to \infty$ at $v \to v_{\rm res}$ (i.e. at $S \to 0$) for the slow wave and $n_\perp$ remains finite for the fast one. The fast mode passes freely through the resonance layer while the slow wave is absorbed or transformed into a hot-plasma mode.

Assume now that the waves are treated using the ray approximation. In the axisymmetrical tokamak geometry, the ray propagation can be considered in the three-dimensional $\{r, \theta, n_\parallel\}$ phase space where r is the 'radial' coordinate labelling the flux surface and θ is the generalized poloidal angle. A ray belongs to one of the mode types which is determined by the initial conditions. This characteristic remains unchanged until the ray reaches the surface $n_\parallel = n_{\rm min}(r, \theta)$ in the phase space where the two roots of the dispersion relation merge or 'intersect'. The normal component of the group velocity vanishes on the surface and its signs are opposite for the two modes in its vicinity. The ray trajectory approaches the conversion surface tangentially and changes its mode label at the touching point, i.e. here it undergoes the linear conversion, see figure 1(*b*). The energy carried by the ray remains unchanged in the event.

The smooth continuous transition between the slow and the fast mode reflects the fact that both belong to the same wave normal surface. In this case, the distinction between the two modes is, in a sense, a matter of convention and depends on the adopted principle of classification. For example, in the variables $\{v_{\rm ph}, \alpha\}$, with α being the angle between the wavevector and the magnetic field, there is only one wave mode described by an unambiguous function $v_{\rm ph}(\alpha)$. This is illustrated by the wave normal surface in figure 2.

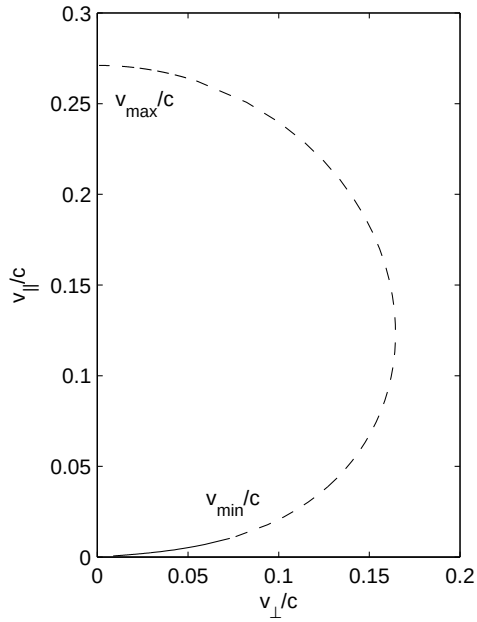

Figure 2. Cross section of the wave normal surface showing the parallel and the perpendicular phase velocity for the fast wave (dashed curve) and the slow wave (full curve) for the parameters of figure 1(*b*). Only one quarter of the cross section having the shape of a figure of eight is shown.

The form and the position of the conversion surface $n_\parallel = n_{\rm min}$ in the phase space are readily understood from equation (2). The function $n_{\rm min}(r, \theta)$ is typically close to unity. It consists

of two branches which merge at the resonance layer. In the absence of the LH resonance, the branches are separated and the lower one having the minus sign lies in the evanescent region.

Consider the conversion process in more detail and begin with the case of the slab geometry discussed intensively in the literature. Suppose that a uniform magnetic field B is in the z-direction and the plasma density $n_{e,i}$ depends only on the x coordinate. Assume also that $\omega < (\Omega_e\Omega_i)^{1/2}$ and the LH resonance layer exists in the plasma. Figure 3(*a*) shows the accessibility regions of the slow and the fast wave in the $\{x, n_\parallel\}$ phase plane. The boundaries of the slow wave domain are the cut-off surface at $v = 1$, the LH resonance layer $v = v_{res}$, and the conversion surface $n_\parallel = n_{min}$. The fast wave region is enclosed by the $n_\parallel = n_{max}(x)$ cut-off and the $n_\parallel = n_{min}(x)$ conversion surfaces. Unlike the slow mode, the fast wave rays can propagate through the LH resonance into the region $v > v_{res}$. The slow and the fast wave domains should be imagined as lying on the opposite sides of a sheet with a transition between them only possible through a cut made along the $n_\parallel = n_{min}$ line.

The rays propagate along horizontal lines in the $\{n_\parallel, x\}$ slab geometry. Therefore, the rays experience the linear conversion if their $n_\parallel$ is in the interval $1 < n_\parallel < n_{GS}$, where $n_{GS} = (1 + w_{res})^{1/2}$ is the maximum value of $n_\parallel$ on the conversion surface and $w_{res} = [(\Omega_e\Omega_i/\omega^2) - 1]^{-1}$. Such rays are locked in the plasma periphery between the edge and the n_{min}-surface and oscillate between these boundaries taking alternatively the form of the slow and the fast mode. Rays having $n_\parallel > n_{GS}$ propagate towards the plasma interior and reach the LH resonance at v_{res}. The inequality $n_\parallel > n_{GS}$ is the well known Golant–Stix condition for accessibility to the LH resonance. The case with no LH resonance within the plasma slab is illustrated in figure 3(*b*).

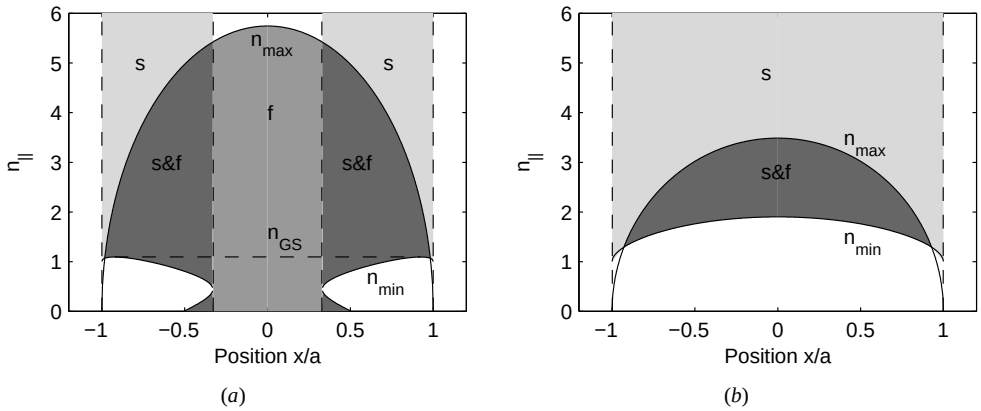

Figure 3. Accessibility regions of the slow (s) and the fast (f) wave in a slab geometry: (*a*) $\omega < \Omega_{LH}$ ($f = \omega/2\pi = 0.6$ GHz, $n_{e0} = 2.2 \times 10^{19}$ m^{-3}) and (*b*) $\omega > \Omega_{LH}$ ($f = 3.7$ GHz, $n_{e0} = 5 \times 10^{19}$ m^{-3}). A deuterium plasma is assumed with the parabolic density profile $n_e(x) = n_{e0}[1 - (x/a)^2]^\beta + n_{e1}$ ($n_{e1} = 1 \times 10^{15}$ m^{-3}, $\beta = 1$, $B = 3.2$ T).

One obvious effect of the toroidal geometry is that $n_\parallel$ is not constant along a ray. As a result, even a ray launched below the Golant–Stix limit can reach the resonance and similarly, a ray having initially $n_\parallel > n_{GS}$ can experience the conversion. In addition, toroidal effects can change the volume and the shape of accessibility regions considerably for both wave modes. The reason lies in the coupling between variations of $n_\parallel$ and the poloidal refractive index n_p [8].

Consider a tokamak with a major radius R_0, minor radius a, poloidal magnetic field B_p and total magnetic field B. Assuming for clarity $(B_p/B)^2$ and a/R_0 to be small, we have

$n_\mathrm{p} = (B/B_\mathrm{p})(n_\parallel - n_{\phi 0})$, where the toroidal refractive index $n_{\phi 0} = c\,\ell/\omega R_0$ is constant along the ray and ℓ is the toroidal mode number. Within the same accuracy, we have $n_\perp = (n_r^2 + n_\mathrm{p}^2)^{1/2}$, where n_r is the radial component of the refractive index. This leads to the condition [8, 10]

$$n_\perp(n_\parallel) \geqslant (B/B_\mathrm{p})|n_\parallel - n_{\phi 0}|. \tag{3}$$

The boundary of the phase-space volume defined by this requirement represents a cut-off surface. Implications of the constraints put on the wave propagation by equation (3) become obvious when both its left-hand and right-hand sides are presented graphically. This is shown in figure 4. In particular, one can see that it is equation (3) rather than the condition $n_\parallel = n_\mathrm{max}$ which actually determines the boundary of the allowed phase space for the fast mode.

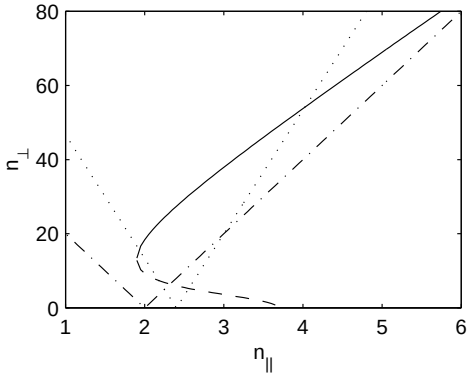

Figure 4. Constraints for the refractive index in a toroidal geometry for the parameters of figure 1(*b*). The dash–dot line shows constraint (3) when $n_{\phi 0} = 2.0$ and $B_\mathrm{p}/B = 0.05$ and the dotted line that when $n_{\phi 0} = 2.4$ and $B_\mathrm{p}/B = 0.03$ ($n_\mathrm{e} = 5 \times 10^{19}$ m^{-3} and $B = 3.2$ T).

From equation (3) a necessary condition for the mode conversion at a given spatial $\{r, \theta\}$ point is readily derived by using the values of $n_\parallel$ and $n_\perp$ at the conversion surface. The result is

$$v^{1/2}(r/qR_0)(w/S)^{1/4} + S^{1/2} + w^{1/2} > n_{\phi 0} \tag{4}$$

where q is the safety factor. The left-hand side of this equation has, as a function of θ, a maximum at the low-field side of the tokamak at $\theta = 0$ and a minimum at $\theta = \pi$. Therefore, the conditions for the mode conversion are most favourable on the low-field side. The conditions also improve with increasing plasma density.

Denoting the maximum value of the left-hand side in equation (4) in the plasma volume as n_c, we obtain the sufficient condition for the absence of mode conversion: $n_{\phi 0} > n_\mathrm{c}$. Under this condition, cut-off always occurs before $n_\parallel$ reaches its limiting value n_min. In this case, the phase-space domains of the two modes are separated by an evanescent region, although they overlap in the coordinate space. Below n_c the domains are connected through a part of the $n_\parallel = n_\mathrm{min}$ surface and mode conversion is possible. It is also clear in figure 4 that the fast wave domain vanishes when $n_{\Phi 0}$ is above the maximum value of n_max. This implies that it is impossible for the mode conversion to occur in this case also.

Evolution of the accessibility conditions with $n_{\phi 0}$ is illustrated in figure 6 where the mode domains are shown in an $\{r, n_\parallel\}$ cross section of the phase space at $\theta = 0$ and $\theta = \pi$, i.e. in the equatorial plane of the tokamak for the case with no LH resonance. It should be noted that the inequality $n_{\phi 0} < n_\mathrm{c}$ is, strictly speaking, the necessary condition for the mode conversion. The answer to the question of whether a real ray actually crosses the conversion surface depends

on the particular solution of the ray equation and cannot be found in advance. One can assume that, due to the stochastic behaviour of the propagation of the small $n_\parallel$ rays, mode conversions are random events which can be treated statistically. This approach is applicable, however, only at a sufficiently low electron temperature where rays survive many reflections before being absorbed. At higher temperatures typical of large tokamaks, the ray-tracing method seems to be, at present, the only reliable tool for investigating mode conversion.

3. Quasitoroidal ray-tracing model

To investigate mode transformations in a simplified geometry, a quasitoroidal axisymmetric tokamak configuration with circular concentric magnetic surfaces is adopted. A magnetic field $\boldsymbol{B} = B_\mathrm{t}\hat{\phi} + B_\mathrm{p}\hat{\theta}$ is assumed, where $\hat{\phi}$ and $\hat{\theta}$ are the unit vectors in the toroidal and poloidal directions, respectively. The toroidal field component is $B_\mathrm{t} = \hat{B}_\mathrm{t}R_0/R$, where $\hat{B}_\mathrm{t} = B_0$ is constant, and R is the major radius coordinate and R_0 its value at the plasma centre. The poloidal component is defined as

$$B_\mathrm{p} = \hat{B}_\mathrm{p}R_0/R$$

where

$$\hat{B}_\mathrm{p} = (\mu_0 I/2\pi)[1 - (1 - r^2/a^2)^{1+\alpha}]/r$$

and I is the total plasma current, r is the minor radius coordinate, a is the minor radius, μ_0 is the vacuum permeability and α is the exponent of the current density profile $j(r) = j_0(1-r^2/a^2)^\alpha$. To describe the wave propagation, a cold plasma is assumed with a radial electron density profile $n_\mathrm{e}(r) = n_{\mathrm{e}0}(1 - r^2/a^2)^\beta + n_{\mathrm{e}1}$. The electron temperature profile was assumed to be $T_\mathrm{e}(r) = T_{\mathrm{e}0}(1 - r^2/a^2)^\gamma + T_{\mathrm{e}1}$.

In the quasitoroidal calculations, we will concentrate on the conditions where the mode transformations occur and we will for the moment ignore the damping of the waves. The damping will be included in section 5, where power deposition is considered.

The wave dispersion is obtained from the zeros of the Hamiltonian in equation (1). The parallel and the perpendicular refractive index components can be obtained from the corresponding toroidal and poloidal mode numbers of the wave which are ℓ and m, respectively. In the given geometry, we find

$$n_\parallel = (\ell/R)(B_\mathrm{t}/B) + (m/r)(B_\mathrm{p}/B) \tag{5}$$

$$n_q = (m/r)(B_\mathrm{t}/B) - (\ell/R)(B_\mathrm{p}/B) \tag{6}$$

with $n_\perp^2 = n_q^2 + n_r^2$. Here, the magnitude of the magnetic field is $B = (B_\mathrm{t}^2 + B_\mathrm{p}^2)^{1/2}$, n_r is the radial component of the refractive index and n_q is the projection of the perpendicular refractive index on the magnetic surface. All the variables here and in what follows are dimensionless: the time has been normalized to ω^{-1} and the length has been normalized to c/ω, where c is the speed of light.

The ray-tracing equations can be written as [4]

$$\mathrm{d}r/\mathrm{d}t = -(\partial H/\partial n_r)/(\partial H/\partial\omega) \tag{7}$$

$$\mathrm{d}\theta/\mathrm{d}t = -(\partial H/\partial m)/(\partial H/\partial\omega) \tag{8}$$

$$\mathrm{d}n_r/\mathrm{d}t = (\partial H/\partial r)/(\partial H/\partial\omega) \tag{9}$$

$$\mathrm{d}m/\mathrm{d}t = (\partial H/\partial\theta)/(\partial H/\partial\omega) \tag{10}$$

which give the rate of change of the polar coordinates r and θ of the ray on the poloidal cross section as well as of the radial refractive index n_r and the poloidal mode number m. Here, the partial derivatives $\partial/\partial n_r$ and $\partial/\partial m$ are obtained from

$$\partial/\partial n_r = (n_r/n_\perp)\partial/\partial n_\perp$$

and

$$\partial/\partial m = (n_q/n_\perp)(B_t/rB)\partial/\partial n_\perp + (B_p/rB)\partial/\partial n_\parallel.$$

The perpendicular refractive index $n_\perp$ is found with the help of n_q and n_r obtained from equations (6) and (9).

The perpendicular refractive index $n_\perp$ solved numerically from the ray-tracing equations can be checked with the help of the solution of equation (1) which is

$$n_\perp^2 = [-F \pm \sqrt{F^2 - 4SC}]/2S. \tag{11}$$

Here, the plus sign corresponds to the slow mode and the minus sign to the fast mode. The values of $n_\perp$ obtained by integrating equations (7)–(10) should coincide with one of the local roots of equation (11).

The wave can propagate only in a region where the expression $F^2 - 4SC$ under the square root is positive, which requirement gives the generalized Golant–Stix condition. A mode transformation happens whenever the ray approaches the point where this expression vanishes, i.e.

$$[(S + P)(n_\parallel^2 - S) + D^2]^2 - 4SP[(S - n_\parallel^2)^2 - D^2] = 0. \tag{12}$$

This region is accessible provided that $-F/2S \geqslant 0$, i.e.

$$(S + P)(S - n_\parallel^2) - D^2 \geqslant 0 \tag{13}$$

which gives a necessary condition for the existence of non-evanescent roots around the mode transformation region. Equation (12) defines surfaces in $(n_\parallel,\ r,\ \theta)$ space, i.e. for each r and θ there can exist real $n_\parallel$ satisfying the condition (12). In a mode transformation, the surface shall be tangential to the ray path at the mode transformation point in phase space.

Mode transformations were investigated by solving equations (7)–(10) for typical launching parameters with the quasitoroidal ray-tracing code (QRTC). The parameters of a JET-like tokamak plasma used in the calculations are presented in table 1 and the parameters of the launched LH spectrum are given in table 2. In simulations with QRTC, the exponent of the current profile was $\alpha = 1$.

Table 1. Plasma parameters in a JET-like tokamak.

Minor radius a (m)	0.95
Major radius R_0 (m)	3.05
Magnetic field B_0 (T)	3.2
Plasma current I (MA)	3.5
Central density n_{e0} (10^{20} m^{-3})	0.6
Edge density n_{e1} (10^{20} m^{-3})	0.001
Exponent of the density profile β	1
Central temperature T_{e0} (keV)	6
Edge temperature T_{e1} (keV)	0.1
Exponent of the temperature profile γ	1.5

In figure 5, the mode polarization is shown along the ray trajectories as well as the mode transformation points. For these example rays, several mode transformations occur—this is partly because the wave damping has been ignored in our quasitoroidal model. Since the slow wave is a backward wave and the fast wave is a forward wave, the radial component of the group velocity of the fast wave is opposite to that of the slow wave at the transformation point. Therefore, whenever the slow wave reaches its transformation point during inward propagation, the fast wave is found to propagate outwards from the transformation point. However, as one

Table 2. Parameters of the lower hybrid spectrum in a JET-like tokamak.

Frequency f (GHz)	3.7
Centre of the spectrum $n_{\phi 0}$	2.0
Width of the spectrum (FWHM) $\Delta n_{\phi 0}$	0.13
Poloidal launching position θ_0 (rad)	± 0.3
Poloidal mode number m_0	0
Radial launching position r_0/a	0.968

can find from figure 5, the fast wave then experiences a reflection from the outer layers with consequent penetration to the plasma centre. The present examples demonstrate how wave partition into fast and slow modes can easily take place for slow modes having access to the plasma centre.

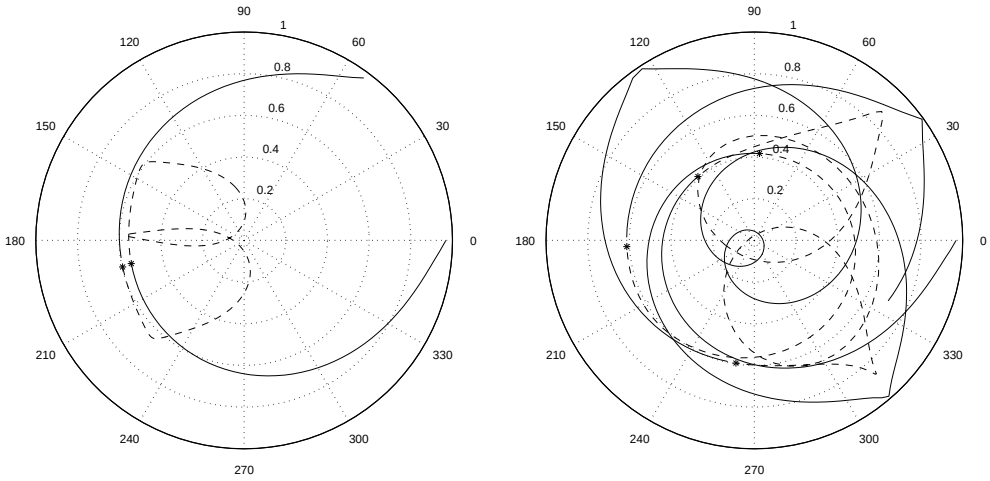

Figure 5. Examples of ray trajectories with transformations (∗) between the slow mode (full curve) and the fast mode (dashed curve) in a JET-like tokamak: (*a*) $n_{\phi 0} = 1.8$ and (*b*) $n_{\phi 0} = 2.0$ ($n_{e0} = 0.5 \times 10^{20}$ m^{-3}, $\theta_0 = 0$).

4. Accessibility conditions for the slow and the fast modes in a torus

In this section we present some numerical results for accessibility conditions in real tokamak plasmas. An exact condition for the coefficients A, F and C of the dispersion relation is written [8, 10] as

$$\left[n_\parallel \sqrt{1 - (B_p/B)^2} - \ell/R \right]^2 \leqslant (B_p/B)^2 n_\perp^2 \tag{14}$$

which is actually just a more accurate version of the simplified equation (3) introduced in section 2.

Figure 6 shows accessibility regions of the slow and the fast waves for different values of the toroidal refractive index $n_{\phi 0}$ in $n_\parallel$–r space along a horizontal radial line through the plasma centre. The plasma parameters are again those of a JET-like tokamak in table 1. The Golant–Stix condition in equation (12) is also depicted. The boundaries shown in figure 6 are

independent of the initial launching parameters m_0 and θ_0, but the actual phase-space region covered by any ray may strongly depend on the chosen initial parameters.

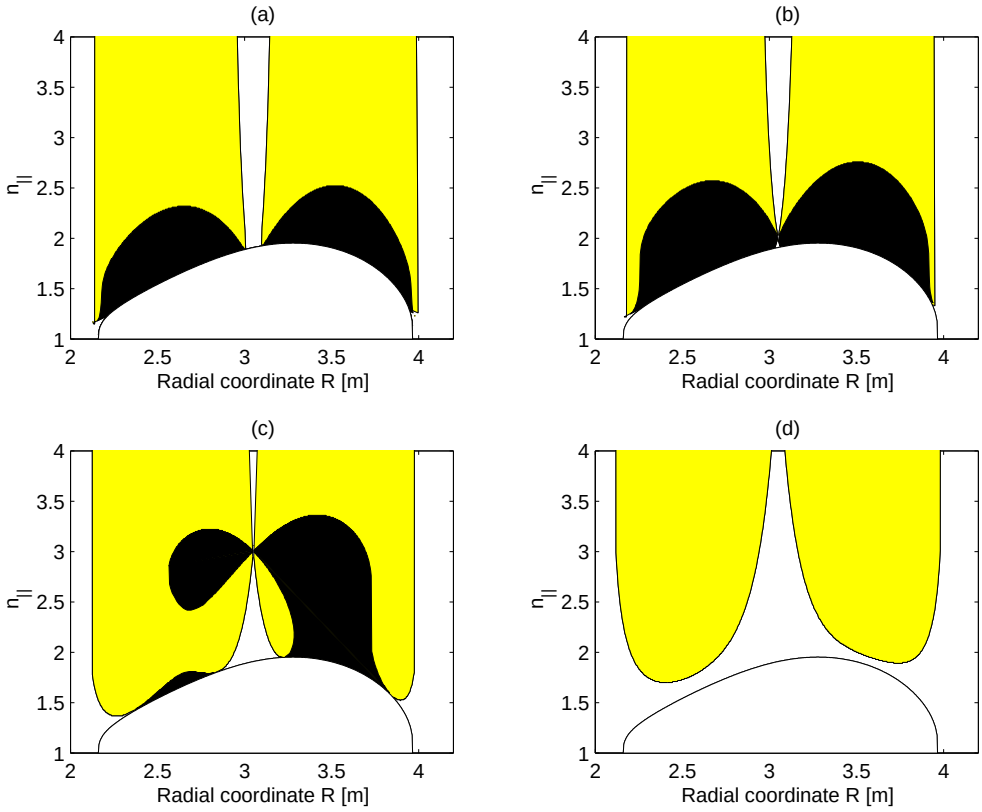

Figure 6. Accessibility regions of the slow wave (grey) and the fast wave (black) in the horizontal plane for a JET-like tokamak. The initial values of the toroidal refractive index are: (*a*) $n_{\phi 0} = 1.6$, (*b*) $n_{\phi 0} = 2.0$, (*c*) $n_{\phi 0} = 3.0$ and (*d*) $n_{\phi 0} = 5.0$ ($n_{e0} = 0.5 \times 10^{20}$ m^{-3}).

The accessibility regions of the slow and the fast waves are found to overlap, but the region of the slow wave is much larger than that of the fast wave. The transformation between the modes is possible only on the Golant–Stix boundary. For sufficiently small toroidal refractive index $n_{\phi 0}$, both the fast and the slow modes appear on this boundary and the transformation is possible. On the other hand, for large $n_{\phi 0} = 5.0$ in figure 6(*d*), the fast mode disappears at the Golant–Stix boundary and no mode transformation is possible. The behaviour obtained is of general nature and implies that the appearance of mode transformations in the plasma interior requires a launched spectrum of $n_{\phi 0}$ to extend below a certain threshold, as noted in [5]. It is of interest to note that the fast waves have access to the plasma centre and do not allow large shift of $n_\parallel$ during propagation.

The values of $n_\parallel$ on the mode transformation surface can be obtained from condition (12) or more simply from equation (2), and here are depicted from equation (2) in r–θ space in figure 7 for two central densities. In order for the ray to reach this surface its $n_\parallel$ has to reduce. The mode transformation surface has a distinct minimum of $n_\parallel$ in the region around $\theta/2\pi = 0.5$, i.e. on the high-field side of the tokamak. Correspondingly, there is a maximum of the surface on the low-field side at $\theta = 0$. In the low-field side, a smaller down shift in $n_\parallel$ is enough to

obtain a mode transformation. Therefore, one could expect that mode transformations occur more often on the low-field side than on the high-field side.

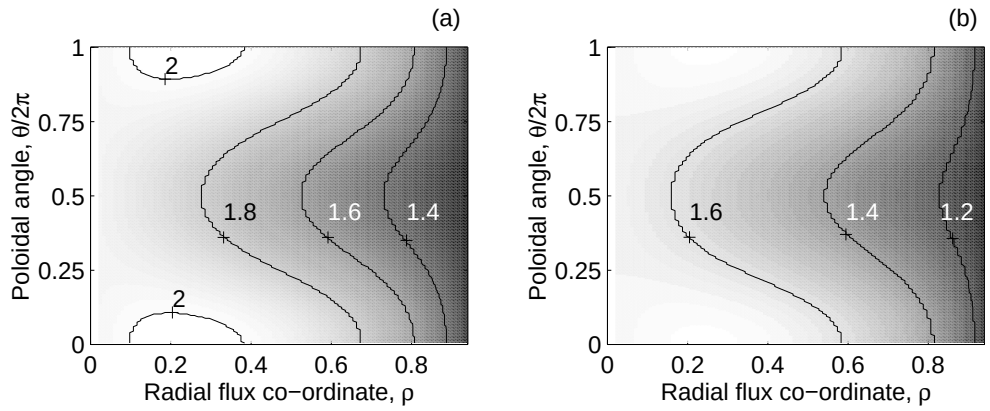

Figure 7. A contour plot of the values of $n_\parallel$ on the mode transformation surface for a JET-like tokamak. The central densities are: (*a*) $n_{e0} = 0.6 \times 10^{20}$ m^{-3} and (*b*) $n_{e0} = 0.3 \times 10^{20}$ m^{-3}.

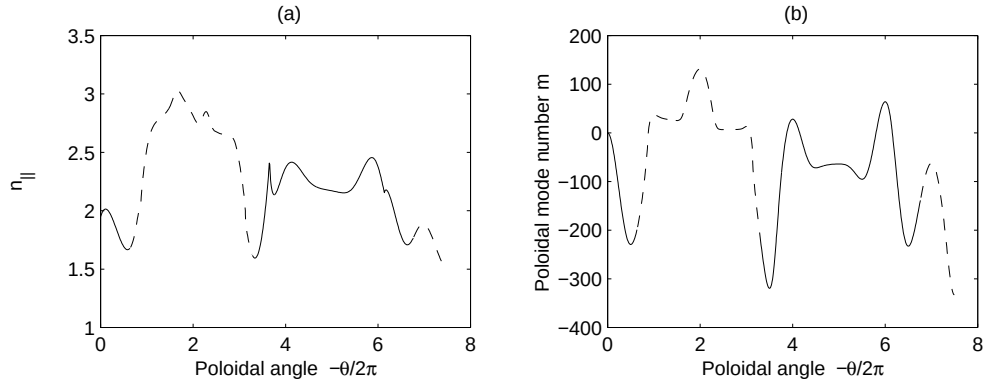

Figure 8. (*a*) The parallel refractive index $n_\parallel$ of the slow wave (full curve) and the fast wave (dashed curve) along a ray as a function of the poloidal angle for a JET-like tokamak. (*b*) The poloidal mode number m along the same ray. Note that this is the same ray as in figure 5(*b*) ($n_{e0} = 0.5 \times 10^{20}$ m^{-3}, $n_{\phi 0} = 2.0$ and $\theta_0 = 0$).

The variation of $n_\parallel$ and the poloidal mode number m along the ray as a function of the poloidal angle θ is shown in figure 8 for the ray we have already presented in figure 5(*b*). The launching point of the ray is at angle $\theta_0 = 0$ and the initial poloidal mode number is $m_0 = 0$. As has been explained in [2], both m and $n_\parallel$ start decreasing for such initial conditions after ray launching. Here, m decreases sufficiently to make $n_\parallel$ so small that a mode transformation occurs at $\theta/2\pi \simeq -0.7$. One can find an estimate for the variation of m from the ray-tracing equations by using the electrostatic approximation [2]

$$\mathrm{d}m/\mathrm{d}\theta = -\frac{\partial H/\partial\theta}{\partial H/\partial m} \approx -n_\parallel R_0 q(r)\left(1 + \frac{\omega_{pe}^2/\Omega_e^2}{S}\right)\frac{(r/R_0)\sin\theta}{1 + (r/R_0)\cos\theta} \qquad (15)$$

where $q(r)$ is the safety factor. Clearly, m reduces for increasing $|\theta|$ when we have $0 < |\theta| < \pi$, and so does $n_\parallel$, which can also be seen in figure 8.

In figure 9, the perpendicular refractive index obtained from ray tracing is depicted for various initial values of the toroidal refractive index. The slow and the fast branches of the dispersion relation along the ray trajectory are also shown. In figure 9(*a*) with $n_{\phi 0} = 1.6$, we find the slow wave to transform to a fast wave at $\theta/2\pi \simeq -0.2$ and $\theta/2\pi \simeq -0.85$, respectively. The transformation back to a slow wave occurs at $\theta/2\pi \simeq -0.3$ and $\theta/2\pi \simeq -0.95$, respectively. At a large value of $n_{\phi 0}$, the transformation does not exist at all in accordance with figure 6.

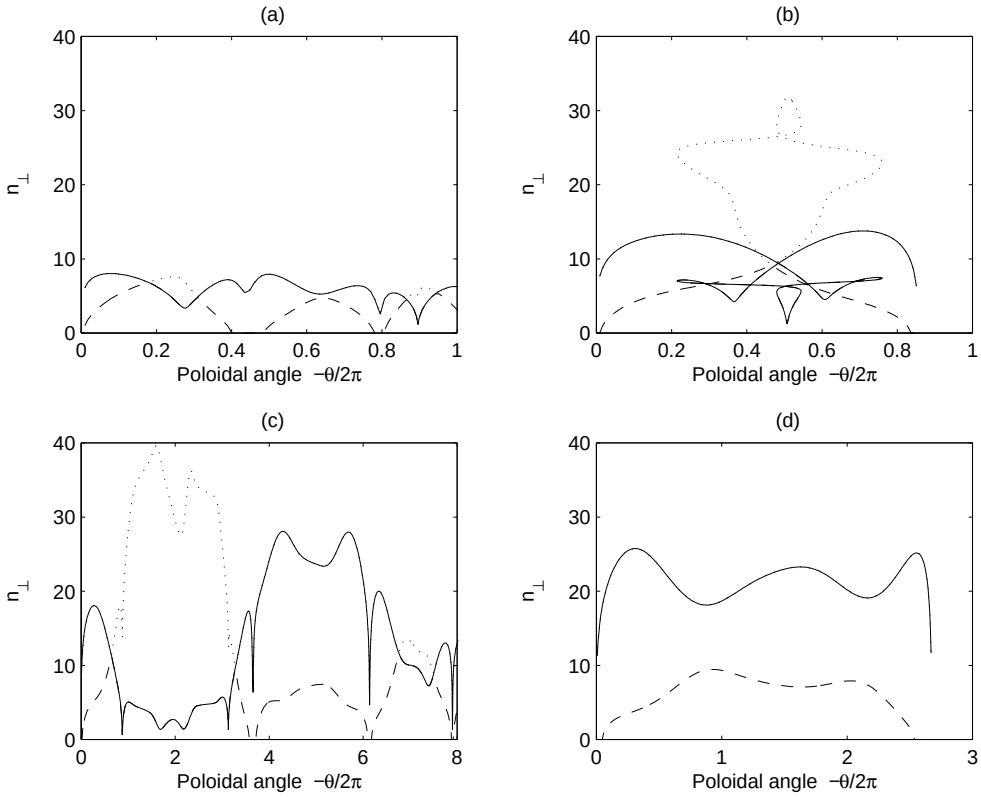

Figure 9. The perpendicular refractive index along a ray (full curve) against the poloidal angle in a JET-like tokamak. The slow branch (dotted curve) and the fast branch (dashed curve) of the dispersion relation are also shown. The initial values of the toroidal refractive index are: (*a*) $n_{\phi 0} = 1.6$, (*b*) $n_{\phi 0} = 1.8$, (*c*) $n_{\phi 0} = 2.0$ and (*d*) $n_{\phi 0} = 2.4$ ($n_{e0} = 0.5 \times 10^{20}$ m^{-3}, $\theta_0 = 0$).

Figure 10 shows the evolution of the perpendicular refractive index at different plasma densities when the toroidal refractive index is $n_{\phi 0} = 2.0$. It seems that the probability of a mode transformation increases when the central density becomes larger. At the lowest central densities below $n_{e0} \simeq 0.3 \times 10^{20}$ m^{-3}, no transformation is found, while at densities above $n_{e0} \simeq 1.0 \times 10^{20}$ m^{-3} the transformation is inevitable. More evidence on enhancement of mode transformation with increasing density will be presented in the following section.

The effect of changing the total current, i.e. changing the edge safety factor $q(a)$, on the fast wave propagation and power deposition was also investigated. The results clearly indicated that the larger the plasma current, i.e. the smaller $q(a)$, the more probable is the mode transformation from the slow to the fast wave. This result can also be deducted from equation (4) where the first term on the left-hand side is larger with smaller q.

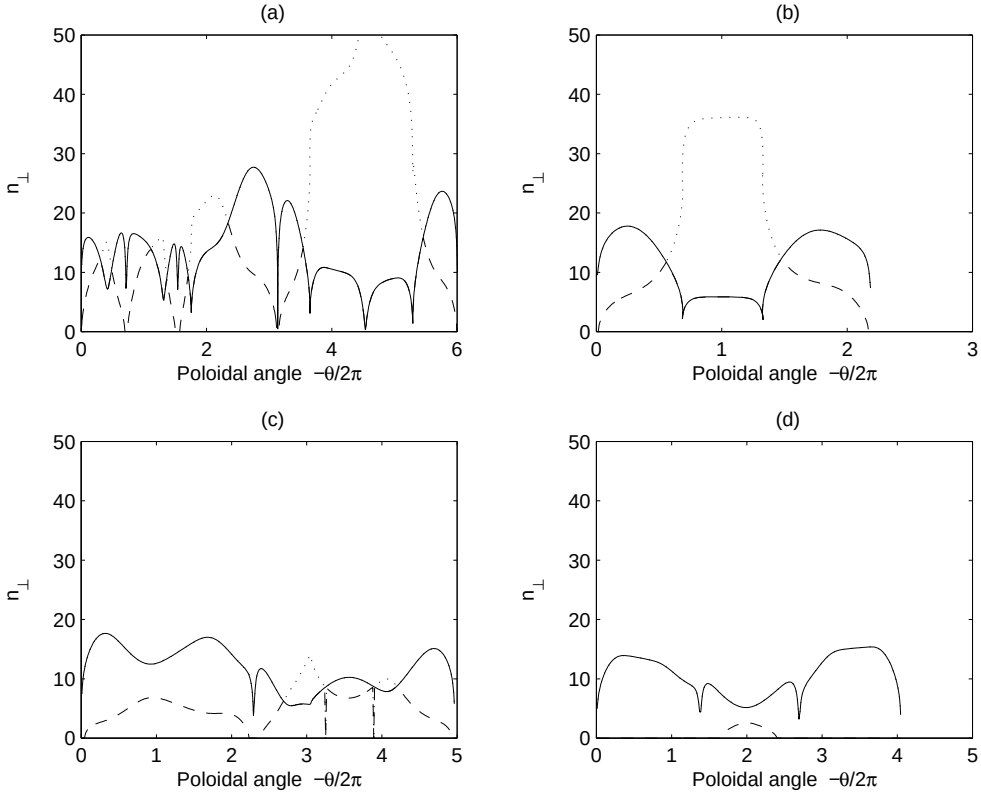

Figure 10. The same as in figure 9, but for different central densities: (*a*) $n_{e0} = 1.0 \times 10^{20}$ m^{-3}, (*b*) $n_{e0} = 0.6 \times 10^{20}$ m^{-3}, (*c*) $n_{e0} = 0.3 \times 10^{20}$ m^{-3} and (*d*) $n_{e0} = 0.1 \times 10^{20}$ m^{-3} ($n_{\phi 0} = 2.0$ and $\theta_0 = 0$).

5. Effect of mode transformation on power deposition

A fast wave has different polarization and smaller $n_\parallel$ during propagation than a slow wave. In general, the electron damping term of a fast wave is similar to that of a slow wave. Assuming that $\omega_{pe}^2/\Omega_e^2 \ll 1$, we find for the imaginary part of the radial refractive index [11]

$$n_{r,i} \simeq n_r \frac{\pi^{1/2}\zeta \exp(-\zeta^2)}{1 + (\Omega_e/\omega_{pe} n_\parallel)^2 (n_\parallel^2 - S)^2} \tag{16}$$

where $n_r \simeq (\omega_{pe}^2/\omega\Omega_e)(n_\parallel^2 - S)^{-1/2}$ and $\zeta = c/(\sqrt{2} v_e n_\parallel)$. For a fast wave, the exponential term is smaller than for a slow wave because the fast wave typically has smaller $n_\parallel$. Since fast waves do not form resonance cones, the weaker absorption disperses the energy in a larger region of plasma. This may improve the penetration, in particular at high densities, where most of the absorption appears to be that of the fast mode.

We now analyse the effect of mode transformation on the power deposition in a JET-like tokamak having the parameters given in tables 1 and 2. In contrast to the previous sections, we now consider a non-circular plasma with elongation $\kappa = 1.74$. We assume that the triangularity is $\delta = 0.4$. The present model for the magnetic equilibrium does not have an X-point. The launched LH power is 6 MW and a deuterium–tritium (50:50) plasma is assumed. The full width of the launched Gaussian spectrum at half maximum is $\Delta n_{\phi 0} = 0.13$.

The power deposition profiles and the current density profiles were calculated with the fast ray-tracing code (FRTC) [9] coupled with the ASTRA transport code. The simulation procedure includes combined ray-tracing and Fokker–Planck calculations. The input RF power is distributed among a number of rays in accordance with the radiated Brambilla spectrum. The rays are traced with canonical ray equations whose Hamiltonian function is given by the left-hand side of the full electromagnetic dispersion relation in the cold plasma approximation. The type of wave mode, specified initially and changing due to the mode transformation, is known at any point of the ray trajectory. The power assigned to individual rays evolves according to Landau and collisional damping. Both the damping rates depend on the current wave polarization that is taken into account in the calculations. For the purpose of this paper, the power depositions into a phase-space volume element from the rays belonging to the fast and slow modes are calculated separately. A one-dimensional model of the Fokker–Planck equation is used with the diffusion coefficient compatible with the assumed damping mechanism. The coefficient is found from the power deposition data. The self-consistent equilibrium between the electron distribution and the power deposition is achieved iterationally. In these calculations, 100 rays were used and fixed density and temperature profiles were assumed with the parameters given in table 1.

The total absorbed power and the power absorbed as a fast wave is illustrated in figure 11. Different values of the toroidal refractive index are considered when the central density is $n_{e0} = 0.5 \times 10^{20}$ m^{-3} and the temperature is $T_{e0} = 6$ keV. As is expected, the amount of mode transformation increases when the initial toroidal refractive index becomes small enough. When we have $1.6 \lesssim n_{\phi 0} \lesssim 2.0$, the contribution of the fast wave to the deposited power is significant and is responsible for the most absorption at the centre. At large values of the toroidal refractive index ($n_{\phi 0} \gtrsim 2.2$), the effect of the fast wave is small.

The observed increase in the fast wave absorption with deceasing toroidal refractive index is in agreement with our results obtained from the quasitoroidal model in section 4. According to figure 6(*d*), the mode transformations are absent at high values of $n_{\phi 0}$ because the fast wave is not accessible. When $n_{\phi 0}$ is large, it was found in figure 9(*d*) that the slow and the fast branches of the dispersion relation are far away from each other, which makes mode transformation unlikely. Furthermore, it is easier for the wave to reach the mode transformation surface of figure 7 if the initial value of the parallel refractive index is not too large.

The effect of the electron temperature on the power deposition profiles is illustrated in figure 12. Here, the LH wave absorption is strongly off-axis because of enhanced Landau damping. The conversion to the fast mode is also reduced, which is caused by the shortened paths of the rays and thus by the reduced probability of the rays to reach the conversion surface. Here, too, the fast wave is responsible for most of the deepest power deposition. As demonstrated in figure 13, the contribution of the fast wave to the deposited power clearly increases with increasing density. At a high central density of $n_{e0} = 0.6 \times 10^{20}$ m^{-3}, most of the central power deposition occurs as a fast wave mode. At low central densities ($n_{e0} \lesssim 0.2 \times 10^{20}$ m^{-3}), all the lower hybrid power is absorbed as a slow wave.

The observed increase in the fast wave deposition with increasing plasma density is in agreement with our discussion in section 2 and with the quasitoroidal results obtained in section 4. The mode transformation surface presented in figure 7 is located at higher values of $n_{\|}$ when the central plasma density is high, which makes a mode transformation more probable. Figure 10 shows that at low densities the fast and the slow branches of the dispersion relation are far away from each other, which makes a mode transformation unlikely. Also, as explained in the context of equation (4), the fast wave has better access to the conversion surface at higher density. However, as is seen in figure 13(*a*), the LH wave penetration is reduced for densities $n_{e0} \gtrsim$

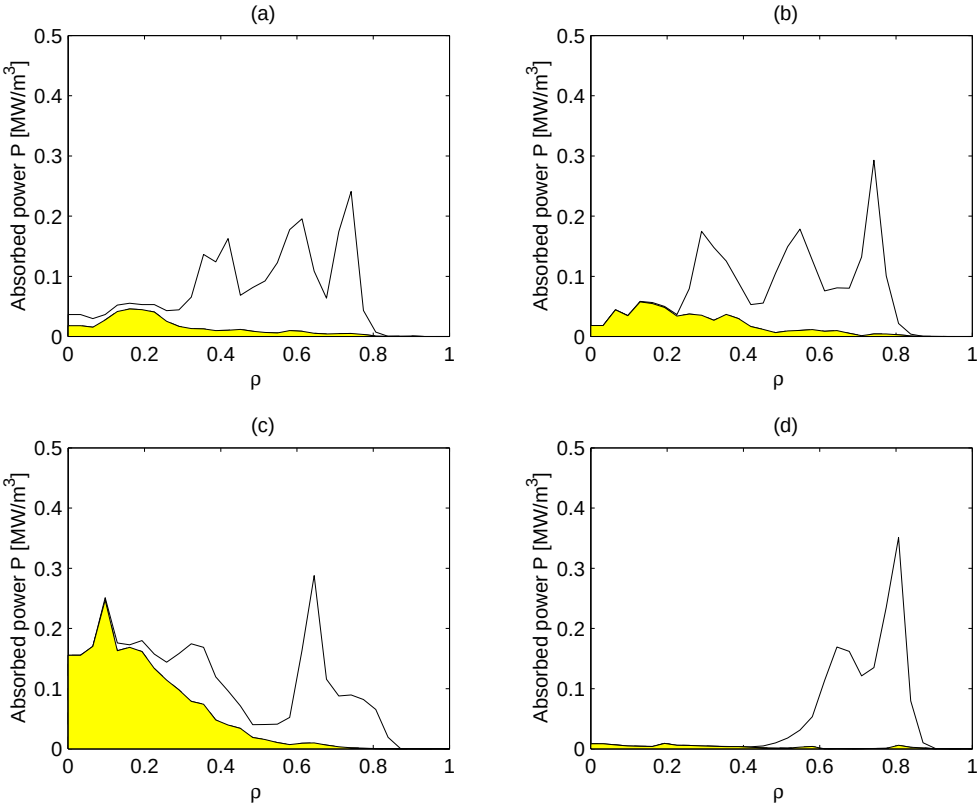

Figure 11. The total absorbed power density and the power density absorbed as a fast wave (shaded) in a JET-like tokamak. The initial values of the toroidal refractive index are: (*a*) $n_{\phi 0} = 1.6$ and (*b*) $n_{\phi 0} = 1.8$, (*c*) $n_{\phi 0} = 2.0$ and (*d*) $n_{\phi 0} = 2.4$ ($n_{e0} = 0.5 \times 10^{20}$ m^{-3}, $T_{e0} = 6$ keV).

1.0×10^{20} m^{-3} which reduces the fast wave contribution as in the case of increased temperature.

It should also be noted that according to equation (15) the variation of m and $n_\parallel$ becomes stronger when ω_{pe}^2/Ω_e^2 becomes larger (provided that $\omega_{pe}^2/\Omega_e^2 \lesssim 1$, as is the case in our examples, except for the highest density $n_{e0} = 1.0 \times 10^{20}$ m^{-3}). Thus, when the density becomes larger (or the magnetic field becomes smaller), the chances increase for the ray to hit the mode transformation surface during propagation.

6. Summary and discussion

The transformation of LH waves from slow waves to fast waves has been investigated in a toroidal configuration. The detailed mechanism of the transformations was first studied with a simple analysis amenable for comparison with the better known slab geometry case. A more detailed analysis was made with a transparent quasitoroidal ray-tracing model. The effect of fast waves on the power deposition profiles in a JET-like configuration was analysed by using the fast ray-tracing code (FRTC).

The effect of the launched spectrum on mode transformation was investigated when the central density was $n_{e0} = 0.6 \times 10^{20}$ m^{-3}. The role of the fast waves is important when the

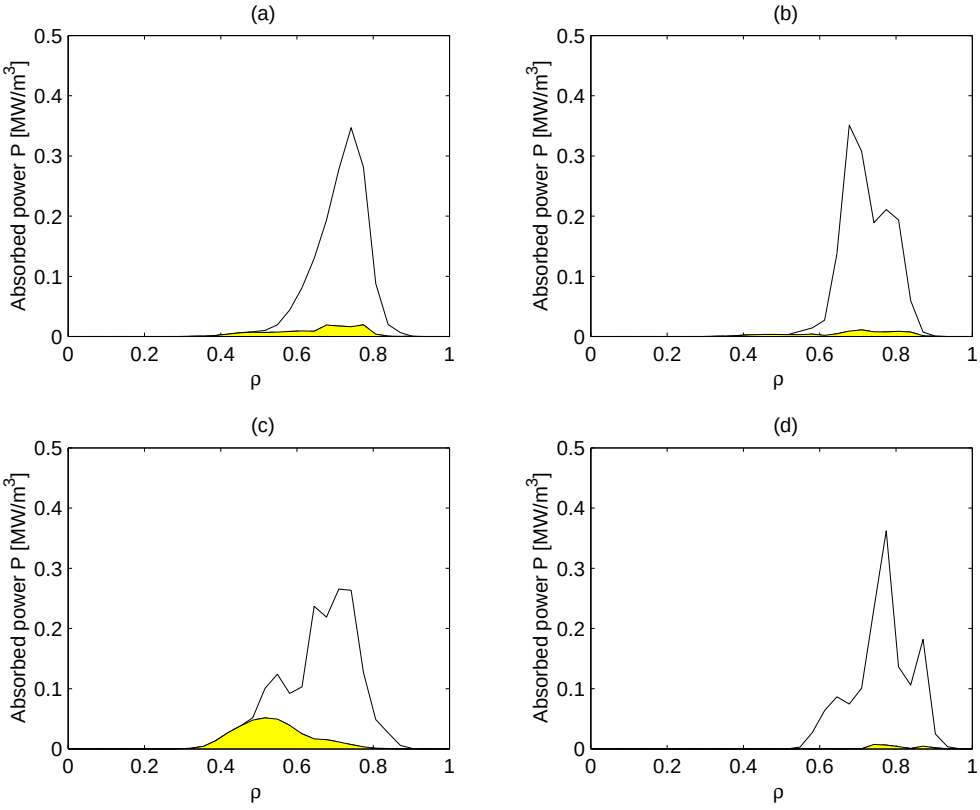

Figure 12. The same as in figure 11 but for a higher temperature of $T_{e0} = 12$ keV.

launched spectrum has small toroidal refractive index $n_{\phi 0}$. If $n_{\phi 0}$ is small ($1.6 \lesssim n_{\phi 0} \lesssim 2.0$), the contribution of the fast wave to the deposited power is found to be even larger than 50% and is responsible for most of the absorption at the centre. On the other hand, if $n_{\phi 0}$ is large ($n_{\phi 0} \gtrsim 2.2$), the effect of the mode transformed fast waves is small or negligible.

The effect of the plasma density was investigated when the toroidal refractive index is $n_{\phi 0} = 2.0$. The contribution of the fast wave to the power deposition also increases with increasing density. At high central densities ($n_{e0} \gtrsim 0.6 \times 10^{20}$ m^{-3}), the contribution of the fast wave to the deposited power can be more than 50%. At low central densities ($n_{e0} \lesssim 0.3 \times 10^{20}$ m^{-3}), practically no absorption of the fast wave occurs. For the highest densities with $\omega_{pe}^2/\Omega_e^2 \gtrsim 1$, the conversion rate is however again reduced because of weakened LH wave penetration and power accessibility to the conversion surface.

Benefits of fast wave for plasma heating and current drive were discussed in [11], where direct launching of fast waves from wave guides was considered. In the present study, the coupling to fast wave occurs via mode transformations. Therefore, the possible advantages of the fast waves are obtained without resorting to a different launching method. Figures 14 and 15 demonstrate the current drive performance of the direct slow and fast wave excitations. In figure 14, the power depositions of the fast and slow wave branches are depicted for various $n_{\phi,0}$ with otherwise similar parameters as in figure 11, but the waves are launched as fast waves. Deepest penetration is found for largest $n_{\phi,0}$ for the fast mode, but here the tunnelling from the antenna across the evanescent layer in the edge plasma becomes more difficult. Comparison

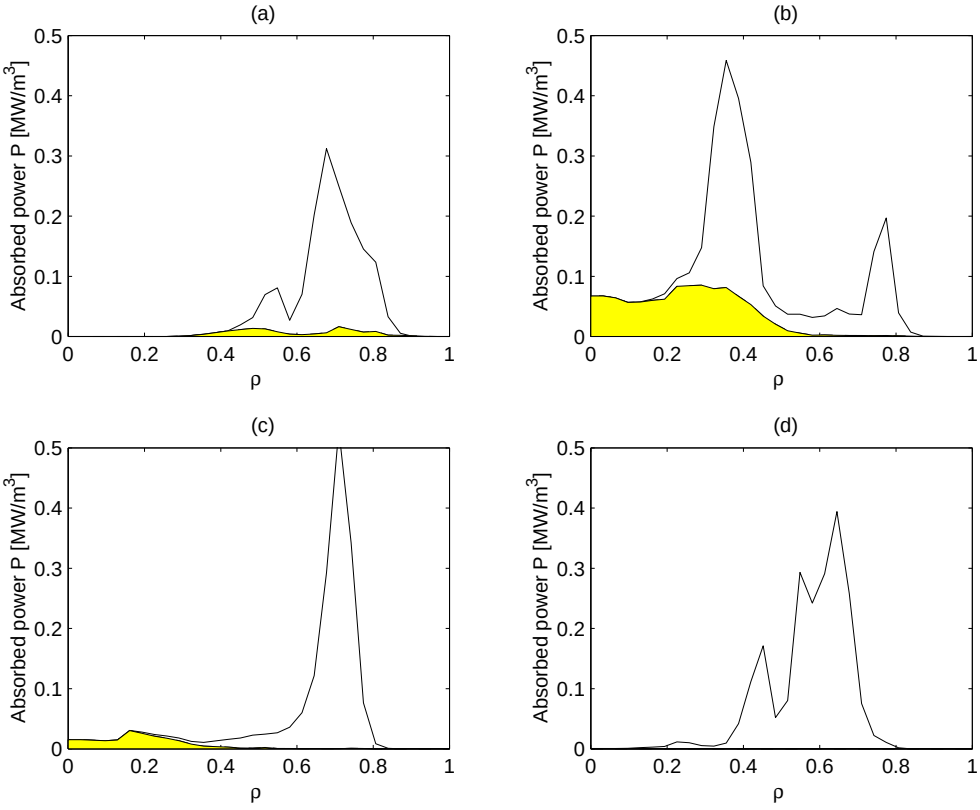

Figure 13. The total absorbed power density and the power density absorbed as a fast wave (shaded) in a JET-like tokamak when $n_{\phi 0} = 2.0$. The central densities are: (*a*) $n_{e0} = 1.0 \times 10^{20}$ m^{-3}, (*b*) $n_{e0} = 0.6 \times 10^{20}$ m^{-3}, (*c*) $n_{e0} = 0.3 \times 10^{20}$ m^{-3} and (*d*) $n_{e0} = 0.1 \times 10^{20}$ m^{-3}.

of figures 11(*c*) and 14(*c*) shows that the relative partition between the fast and slow wave power deposition is very similar. The corresponding driven current profiles in figure 15 show also a fair similarity. Noting the large contribution of the fast wave mode in this case even with a slow wave direct excitation, leads us to conclude that it is possible to achieve some of the advantages of direct fast wave excitation with the present slow wave launchers.

At the highest plasma densities ($n_{e0} \gtrsim 1 \times 10^{20}$ m^{-3}) studied in the present paper, the deposition profiles are off-axis at $\rho \simeq 0.5$–0.8. Thus, neither the fast waves nor the slow waves appear to penetrate to the plasma centre. This demonstrates that the damping of the fast waves can also be strong in the outer plasma layers, thus preventing deep penetration in our examples. As this was found to be a consequence of condition $\omega_{pe}^2/\Omega_e^2 \gtrsim 1$, increasing the magnetic field up to 5 T in a reactor would eliminate this effect for densities around 10^{20} m^{-3}.

The FRTC code has very recently been installed and coupled into the JETTO transport code [12] at JET. FRTC can also be run as a stand-alone version using experimental profiles. Thus, in the future we can use the JET experimental database to simulate the fast wave deposition profiles, and what is even more intriguing are the self-consistent simulations with the coupled JETTO/FRTC transport code. The results of the modelling of LHCD deposition profiles with the coupled JETTO/FRTC code are deferred to future publications.

The significant amount of wave energy in the fast mode must be carefully taken into account in modelling LH current drive experiments. It may have an effect, for instance, on the

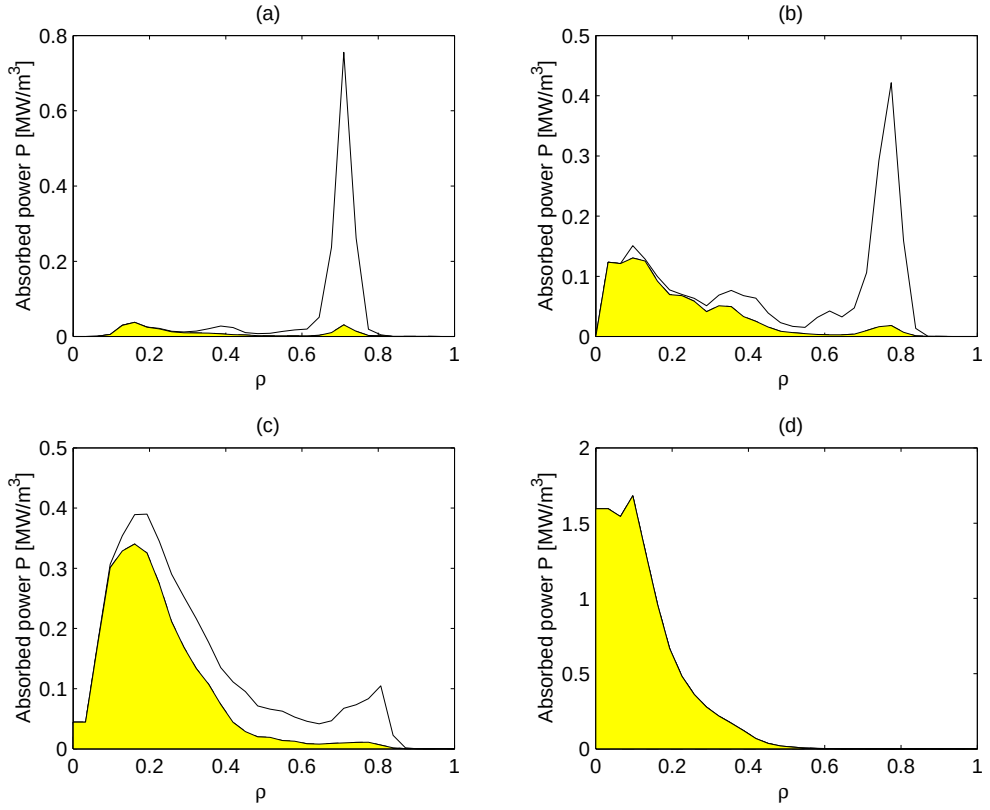

Figure 14. The total absorbed power density and the power density absorbed as a fast wave (shaded) in a JET-like tokamak when the wave is initially launched as a fast wave. The initial values of the toroidal refractive index are: (*a*) $n_{\phi 0} = 1.6$ and (*b*) $n_{\phi 0} = 1.8$, (*c*) $n_{\phi 0} = 2.0$ and (*d*) $n_{\phi 0} = 2.4$ ($n_{e0} = 0.5 \times 10^{20}$ m^{-3}, $T_{e0} = 6$ keV).

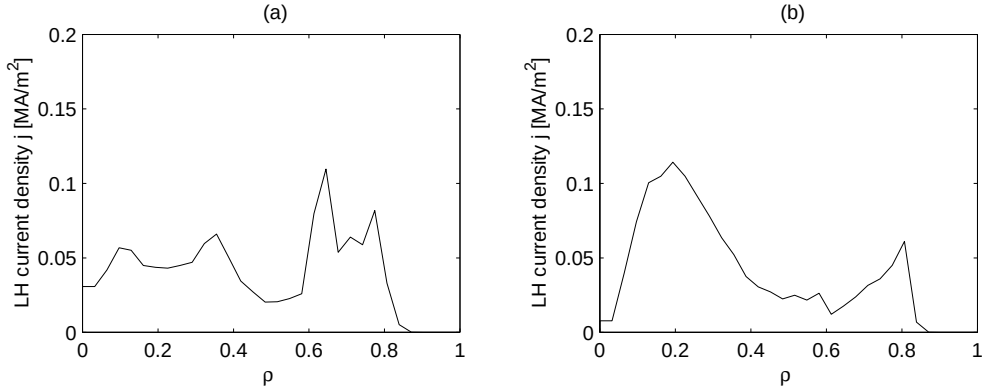

Figure 15. The wave-induced current when the wave is launched (*a*) as a slow wave and (*b*) as a fast wave ($n_{\phi 0} = 2.0$, $n_{e0} = 0.5 \times 10^{20}$ m^{-3}, $T_{e0} = 6$ keV).

absorption of the LH waves by alpha particles and fast ions, the diagnostics of the LH waves and various models of the spectral gap problem. Further work is needed to clarify these issues.

Recently, experimental evidence of LHCD on the PBX-M tokamak was demonstrated although the launched spectrum was below the accessibility condition [13]. It was found that in this case the current drive efficiency decreased with decreasing $n_{\phi 0}$. The reason for this seemed to be that a large spectral upshift was necessary before the absorption could occur. Furthermore, it was found that the damping location was not correlated to accessibility, but to upshift, which was largely independent of the original $n_{\phi 0}$.

The validity of the WKB approximation in the lower hybrid range of frequencies has been critically discussed by several authors [14–17]. In the present work, a well established routine for LHCD simulation has been used. The routine is based completely on commonly accepted, although not always well justified, approaches. A detailed discussion of the validity of the WKBJ approximation for LHCD is, however, beyond the scope of this paper.

Acknowledgments

The authors thank an anonymous referee for bringing the recent results on PBX-M [13] to our attention. The authors are grateful to Karin Rantamäki, Lic. Tech., for technical assistance.

References

[1] Stix T H 1992 *Waves in Plasmas* (New York: AIP) p 101
[2] Bonoli P T and Ott E 1982 *Phys. Fluids* **25** 359
[3] Santini F 1985 *Course and Workshop on Applications of RF Waves to Tokamak Plasmas (Varenna, September 1985)* vol 1, ed S Bernabei, U Gasparino and E Sindoni (International School of Plasma Physics 'Piero Caldirola') (Perugia: Monotypia Franchi, Città di Castello) p 251
[4] Valeo E J and Eder D C 1985 *Course and Workshop on Applications of RF Waves to Tokamak Plasmas (Varenna, September 1985)* vol 2, ed S Bernabei, U Gasparino and E Sindoni (International School of Plasma Physics 'Piero Caldirola') (Perugia: Monotypia Franchi, Città di Castello) p 493
[5] Esterkin A R and Piliya A D 1992 *Plasma Phys. Control. Fusion* **34** 1957
[6] Esterkin A R and Piliya A D 1992 *Nucl. Fusion* **32** 927
[7] Kupfer K and Moreau D 1992 *Nucl. Fusion* **32** 1845
[8] Paoletti F, Ignat D W, Kesner J, Bernabei S, Kaita R, Leblanc B, Levinton F M and Luckhardt S C 1994 *Nucl. Fusion* **34** 771
[9] Esterkin A R and Piliya A D 1996 *Nucl. Fusion* **36** 1501
[10] Wégrove J-G 1997 *Proc. 12th Topical Conf. on Radio Frequency Power to Plasmas (Savannah, GA, April, 1997) (AIP Conference Proceedings vol 403)* (New York: AIP) p 141
[11] Theilhaber K and Bers A 1980 *Nucl. Fusion* **20** 547
[12] Genacchi G and Taroni A 1988 JETTO: A free boundary plasma transport code (basic version) *Rapporto* ENEA RT/TIB 1988(5)
[13] Bernabei S, Cardinali A, Giruzzi G, Hoang G T, Ignat D, Kaita R, Okabayashi M, Paoletti F and von Goeler S 1997 *Phys. Plasmas* **4** 125
[14] Brambilla M and Cardinali A. 1982 *Plasma Phys. Control. Fusion* **24** 1187
[15] Esterkin A R, Gusakov E Z, Irzak M A and Piliya A D 1995 *Proc. 22nd European Physical Society Conf. on Controlled Fusion and Plasma Physics (Bournemouth, 3–7 July, 1995) (Europhysics Conference Abstracts vol 19C)* (Geneva: EPS) part IV, p 389
[16] Peysson Y, Sébelin E, Litaudon X and Moreau D 1998 *Nucl. Fusion* **38** 939
[17] Pereverzev G V 1998 *Phys. Plasmas* **5** 3529